

Sample-shape dependent energy levels in organic semiconductors

Syed A. Abd-Rahman,¹ Takuma Yamaguchi,^{2,3} Satoshi Kera,^{2,3} and Hiroyuki Yoshida^{4,5,*}

¹Graduate School of Science and Engineering, Chiba University, 1–33 Yayoi-cho, Inage-ku, Chiba 263–8522, Japan

²Graduate University for Advanced Studies, SOKENDAI, Shonan Village, Hayama, Mura, Kanagawa 240-0193, Japan

³Institute for Molecular Science, Nishigonaka Myodaijicho, Okazaki, Aichi 444–8585, Japan

⁴Graduate School of Engineering, Chiba University, 1–33 Yayoi-cho, Inage-ku, Chiba 263–8522, Japan

⁵Molecular Chirality Research Centre, Chiba University, 1–33 Yayoi-cho, Inage-ku, Chiba 263–8522, Japan



(Received 11 April 2022; revised 5 June 2022; accepted 28 June 2022; published 15 August 2022)

Energy levels in an organic semiconductor are mainly determined by the molecular orbital energies of the constituent molecules. Recent studies, however, have revealed that the energy levels can be altered as much as 1 eV by the molecular orientation in the film or the molecular mixing ratio in the binary film, owing to the intermolecular electrostatic interaction. Because of the long-range nature of Coulomb interaction, theory predicts that the electrostatic energy should depend on the sample shape. In this article, we examine the coverage-dependent energy levels of zinc phthalocyanine and per-fluorinated zinc phthalocyanine in the submonolayer region with ultraviolet photoelectron spectroscopy (UPS) and low-energy inverse photoelectron spectroscopy (LEIPS). Using the procedure we reported previously, we separately evaluated the electronic polarization energy and electrostatic energy as a function of coverage. Unlike the electronic polarization, which contributes only as much as 10 meV, the electrostatic energy contributes as much as 120 meV to the coverage-dependent energy shift. We conclude that the shift in energy levels by changing the coverage is attributed to the sample shape-dependent energy level, owing to the long-range nature of the charge–permanent quadrupole interaction.

DOI: [10.1103/PhysRevB.106.075303](https://doi.org/10.1103/PhysRevB.106.075303)

I. INTRODUCTION

Ionization energy (I_s) and electron affinity (A_s) of organic semiconductors represent electronic energy levels of the highest occupied molecular orbital (HOMO) and the lowest unoccupied molecular orbital (LUMO) of organic solids, respectively. These two electronic energy levels are one of the performance-determining factors of organic devices, such as organic light-emitting diodes (OLEDs), organic field-effect transistors (OFETs), and organic solar cells (OSCs) [1–5]. For example, increasing the I_s and A_s via halogenation is usually done to facilitate the electron injection into the OLEDs' emissive layer [6,7]. While in OSCs, the open-circuit voltage is limited by the effective gap between the A_s of the acceptor and the I_s of the donor [5]. Furthermore, increasing the I_s and A_s via designing an oligomeric material with heteroatoms such as sulfur, nitrogen, or oxygen atoms, is reported to increase the stability of OFET devices [8–10].

Most of the tuning of the I_s and A_s was done by changing the constituent molecules that are used in the device. This is because the organic solids consist of organic molecules bound by weak interactions such as van der Waals forces. Thus, the energy levels of organic solids are predominantly determined by the molecular orbital energies, whereas the intermolecular interaction is considered to play a minor role. The contribution of the intermolecular interaction to the energy levels of organic solids is represented by the difference in the energy

levels between the gas and solid phases. Historically, the energy difference has been called polarization energy P_{\pm} (the subscript + and – correspond to I and A , respectively) [11]. The fact that most organic solids possess a similar polarization energy of 1 to 2 eV [12] further ensures the importance of the molecular orbital energy to the energy levels in the solid phase.

However, it has been reported recently that the energy levels can be changed up to 1 eV by changing the molecular orientation of the system [13–17] and by varying the mixing ratio of a blend film [18–21]. These changes can be explained by using polarization energy. The polarization energy is contributed by the electronic polarization (dynamic or induction) and the electrostatic effects. The electronic polarization energy is the stabilization energy of the charge carrier due to the electronic polarization of neighboring molecules, and can be approximated by the charge-induced dipole interaction. Electrostatic energy is an interaction between the charge carrier and the permanent charge distribution over the neighboring neutral molecules, approximated by the charge–permanent multipole. It has been established that the electrostatic effect is the main driving force for these orientation and mixing ratio dependencies of the energy levels. The electronic polarization energy, on the other hand, is mostly unchanged.

Theoretically, it is well known that the electrostatic energy depends on the macroscopic shape of the system due to the long-range nature of Coulomb interaction [22–25]. For example, proper calculation of the Madelung constant is still a subject of active research [25]. For the electrostatic energy in organic solids mentioned earlier, the leading term of the elec-

*hyoshida@chiba-u.jp

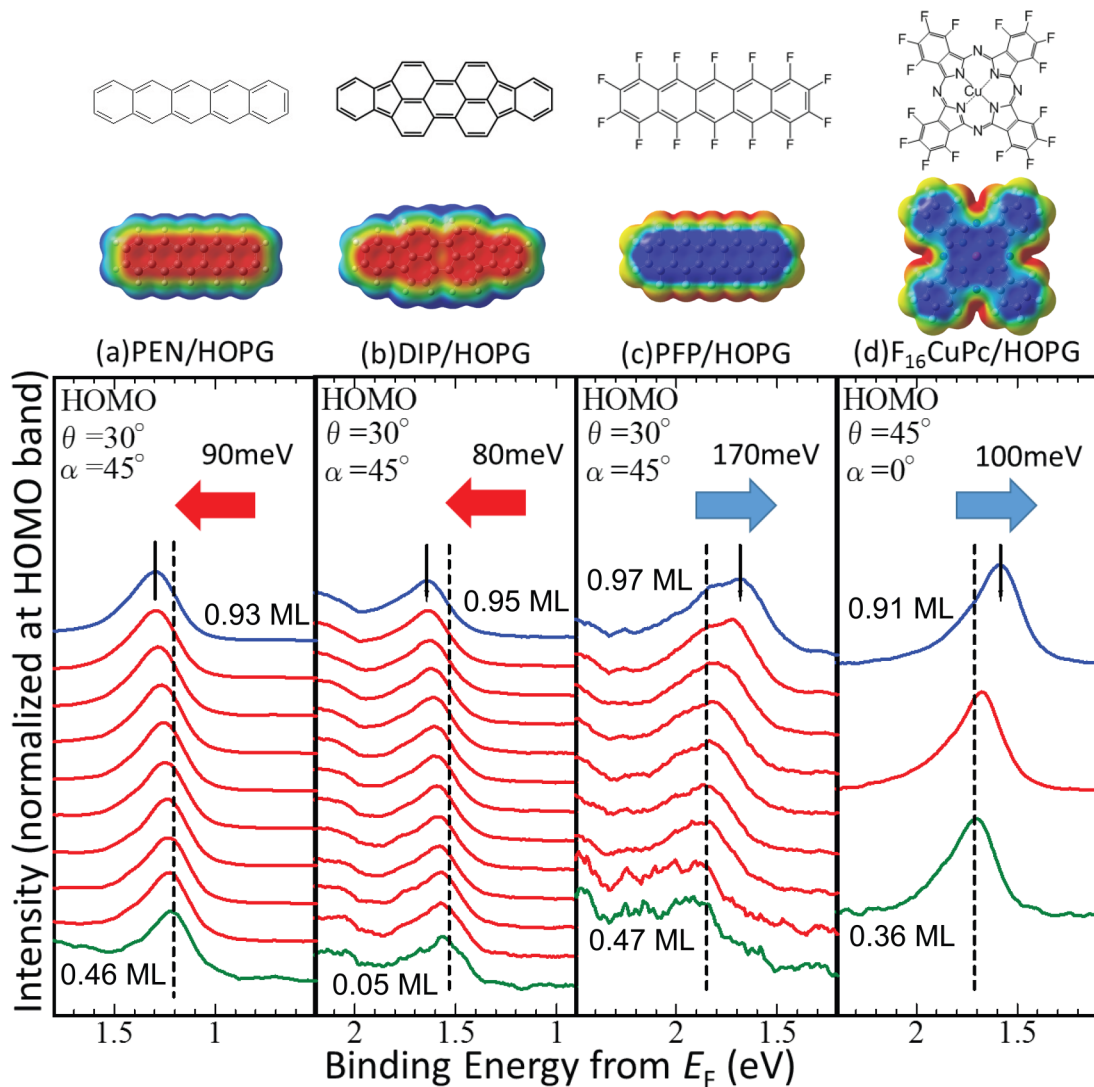


FIG. 1. Coverage dependent UPS spectra for the submonolayer region of (a) pentacene (PEN), (b) diindenoperylene (DIP), (c) perfluoropentacene (PFP), and (d) perfluoro copper-phthalocyanine ($F_{16}CuPc$) in respect with energy from Fermi level (E_F). The green, red, and blue spectra represent the spectra of the sample with the lowest, middle, and highest coverage, respectively. The numbers indicate the coverage in the unit of monolayer (ML). The molecular structure of each molecule is shown on top, along with its charge distribution. The electron density was calculated by density functional theory (B3LYP/cc-PVDZ). The blue and red regions correspond to the positive and negative charges, respectively.

trostatic energy is the charge-quadrupole moment; nonpolar molecules naturally hold this condition, and polar molecules usually crystallize into a noncentrosymmetric crystal structure canceling the permanent dipoles. As the distance r increases, the charge-permanent quadrupole energy decreases as r^{-3} . In the three-dimensional system, the volume integral increases as $r^2 dr$, resulting in a logarithmic dependence of the electrostatic energy, $\log(r)$, while in the two-dimensional system, the volume integral increases as $r dr$, resulting in very slow convergence depending on r [22,24]. This means that the energy levels of the organic semiconductor should depend on the macroscopic shape of the sample. So far, however, no such experimental evidence has been reported.

It has been known that the I_s measured by ultraviolet photoelectron spectroscopy (UPS) depends on the surface coverage below the monolayer thickness [21,26,27]. Figure 1 exemplifies the experimental observations of the coverage-dependent

UPS spectra. As the coverage increases, the I_s changes by about 0.1 eV. The origin of such a coverage-dependent energy shift was not clear; it has often been interpreted as the electronic polarization of neighboring molecules [26] or a coverage-dependent structural change [27]. Recently, Schwarze *et al.* [21] systematically examined the relationship between the energy shift and the molecular quadrupole moment and pointed out that the electrostatic energy generated by the molecular quadrupole moment plays some role in the energy shift. This explanation was still inconclusive because other compelling factors besides the electrostatic energy, such as electronic polarization, cannot be excluded.

The electrostatic energy and electronic polarization energy can be separated based on their opposite response to the negative and positive charges. For this purpose, we need both P_+ and P_- . Only the polarization energy for the positive charge (hole) P_+ can be derived from the previous

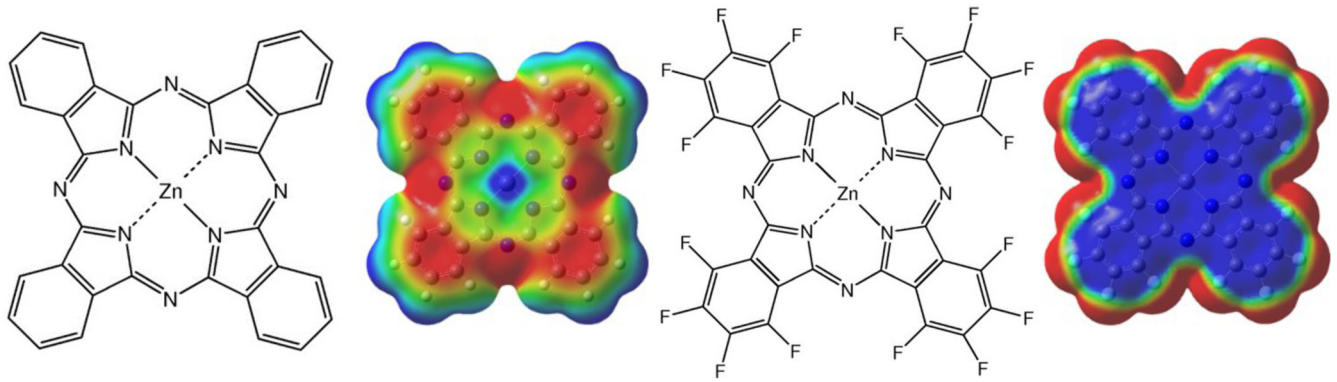


FIG. 2. The molecular structure and surface potential of ZnPc (left) and F_{16} ZnPc (right). Blue and red correspond to the positive and negative charges, respectively. The calculation was made by density functional theory (UBL3LYP/cc-PVDZ).

UPS studies [12–15,17–19,21]. To obtain the polarization energy for the negative charge (electron) P_- , precisely determined A_s is indispensable, which was enabled by the development of low-energy inverse photoelectron spectroscopy (LEIPS) by Yoshida [28,29]. From the observed P_+ and P_- by using both UPS and LEIPS, respectively, we have quantified the electrostatic energy and the electronic polarization energy and elucidated the origin of the orientation-dependent energy levels in thin films [30,31], the mixing ratio dependence of energy levels in binary films [32], and the metal screening effect at the metal/organic interface [33].

In this work, we applied this procedure to investigate the coverage dependent-energy shift. We chose zinc-phthalocyanine (ZnPc) and perfluoro zinc-phthalocyanine (F_{16} ZnPc) due to their opposite quadrupole moment from each other (Fig. 2) to highlight the contribution of electrostatic energy. We quantified both electrostatic energy and electronic polarization energy. The observation clearly shows that the energy shift originates from the electrostatic energy. We calculated the electronic polarization and electrostatic energies for further confirmation by approximating them by charge-induced dipole and charge-permanent quadrupole energies, respectively. During the film growth in the submonolayer region, islands are usually formed. The increase of the surface coverage toward one monolayer is associated with the increase in the island size. We demonstrate that the observed coverage dependence can be interpreted as the electrostatic energy depending on the shape of the sample owing to the long-range nature of Coulomb interaction as predicted in previous theoretical studies [22,24].

II. EXPERIMENTAL METHODS

Highly oriented pyrolytic graphite (HOPG) was used as a substrate. HOPG cleaved in ambient air was introduced into a vacuum chamber with a pressure less than 5×10^{-8} Pa, and the surface was cleaned by heating at 800 K for a minimum of 28 hours. The substrate was cooled to room temperature prior to use. The surface quality of HOPG was evaluated from the σ^* peak observed by a metastable atom electron spectroscopy (MAES) [34,35] measurement (see Supplemental Material Figure S1 [36]). ZnPc and F_{16} ZnPc were purchased from Sigma Aldrich and purified twice by thermal-gradient vacuum

sublimation. The molecules were deposited on HOPG with a deposition rate of 0.15 monolayer (ML) min^{-1} in a vacuum chamber with a pressure of 3×10^{-7} Pa. The deposition process was monitored by quartz crystal microbalance.

The details of the experimental setup are stated elsewhere [37]. UPS was performed first to measure the I_s , followed by LEIPS for A_s , and then UPS was remeasured to check the sample damage from the LEIPS measurement. As no discernible change in the UPS spectra before and after the LEIPS measurement was noticed, we concluded that no damage was inflicted to the sample during the LEIPS measurement. The sample was kept under UHV during all the measurements. One ML thickness was determined by MAES (see Supplemental Material [36]).

UPS was conducted using He I radiation (21.22 eV) for excitation, and the photoelectron kinetic energies were analyzed with the Phoibos100(SPECS) hemispherical electron analyzer. I_s was determined from the HOMO peak observed by the UPS with reference to the vacuum level (E_{vac}). The E_{vac} was determined by the cutoff of the secondary electron. LEIPS was performed in the same apparatus. Details are described elsewhere [38]. Electrons from an Erdmann–Zipf-type electron gun were incident to the sample surface. A bias voltage was applied to the electron gun with reference to the sample to control the kinetic energy of the introduced electron. The LEIPS spectrum was obtained by detecting the photon signal using a photon detector consisting of the bandpass filter with a center energy of 4.785 eV and a photomultiplier tube. A_s was determined from the maximum of the peak assigned to the LUMO-derived feature. The vacuum level was determined from the inflection point of the rising edge of the sample current.

III. RESULTS

The coverage dependence of UPS and LEIPS spectra is shown in Fig. 3. Usually, the I_s and A_s values of a multilayer film are determined by the onsets of the HOMO- and LUMO-derived peaks, respectively. In this study, the I_s and A_s values were taken from the maxima of the HOMO and LUMO peaks because the sample film is thinner than monolayer. The I_s and A_s of ZnPc increase toward the monolayer from 5.56 eV to 5.71 eV and from 3.07 eV to 3.25 eV, respectively; whereas

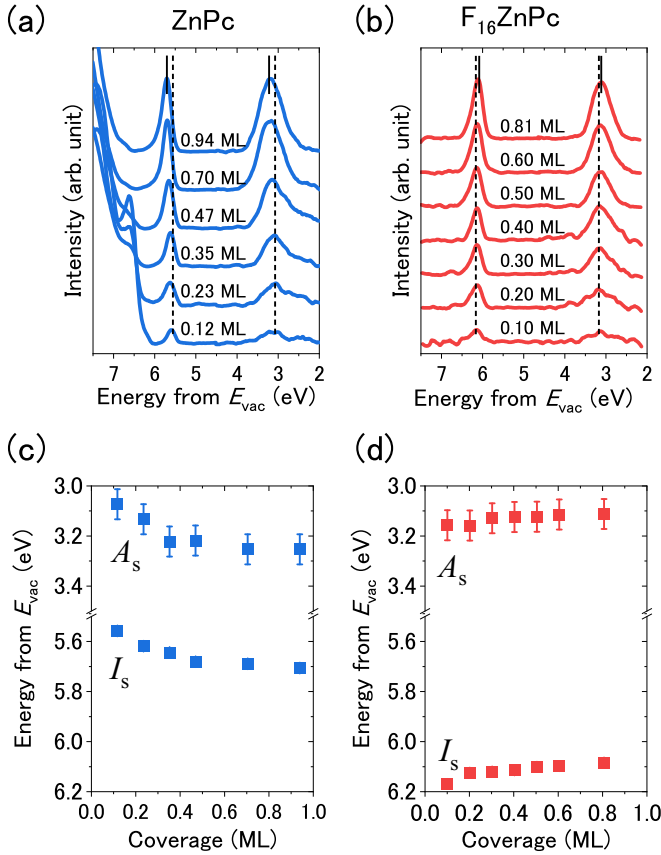


FIG. 3. Combined UPS and LEIPS spectra of (a) ZnPc and (b) F_{16} ZnPc showing the HOMO and LUMO peaks. The peak maxima for the lowest and highest coverage are indicated with dashed and solid lines, respectively. The coverage is indicated between HOMO and LUMO peaks. The determined I_s and A_s for ZnPc and F_{16} ZnPc are shown in (c) and (d), respectively.

for F_{16} ZnPc, the I_s and A_s decrease from 6.17 eV to 6.08 eV and from 3.16 eV to 3.11 eV, respectively. The bandgap ($I_s - A_s$) is almost independent of the coverage, implying that the electronic polarization may not contribute to the coverage dependence. Conversely, the opposite shift direction of the coverage-dependent energy level for ZnPc and F_{16} ZnPc indicates that the shift originated from the electrostatic energy. The systematic error bar was taken from the standard deviation from multiple UPS and LEIPS measurements. The systematic error bar for I_s and A_s is estimated to be 0.02 and 0.06 eV, respectively. Note that I_s and A_s vary by 0.6 eV, depending on the molecular orientation [14,32]. The observed I_s and A_s are consistent with the face-on orientations of ZnPc and F_{16} ZnPc [32].

IV. DISCUSSION

The polarization energies, P_+ for cation and P_- for anion, are expressed as [16]

$$\begin{aligned} P_+ &= I_g - I_s - \Delta_+ \\ P_- &= -A_g + A_s - \Delta_-, \end{aligned} \quad (1)$$

where they are the ionization energy I_g and electron affinity A_g in the gas phase, and the Δ_+ and Δ_- are corrections from the HOMO and LUMO bandwidths, respectively, owing to the intermolecular quantum mechanical electronic couplings. The polarization energy can be the sum of the electronic polarization energy (D) and electrostatic energy (S):

$$\begin{aligned} P_+ &= D_+ + S_+ \\ P_- &= D_- + S_-. \end{aligned} \quad (2)$$

The electronic polarization energy, also referred to as induction or dynamic energy (D), will always stabilize the system regardless of the polarity of the introduced charge (positive/cation for the hole or negative/anion for the electron); we can approximate $D_+ = D_- \equiv D$, where the + and - subscript indicate the polarity of the charge. In contrast, electrostatic energy S is the Coulomb interaction between the introduced charge and the permanent charge distribution of the neighboring neutral molecules. Since the magnitude of S is the total Coulomb potential for all the charges in the system, changing the introduced charge will result in inverted polarity and can be approximated as $S_+ = -S_- \equiv S$. In this approximation, we implicitly assume similar charge distributions between the cation and anion. It should hold because the HOMO and LUMO of phthalocyanines possess a similar distribution of the π -orbital over the molecule.

Due to this difference in nature of both energies, D and S can be evaluated from the measured energy parameters I_s , A_s , I_g , and A_g , by combining Eqs. (1) and (2) [30–33]:

$$\begin{aligned} D &= \frac{I_g - A_g - (I_s - A_s) - \Delta_+ - \Delta_-}{2} \\ S &= \frac{I_g + A_g - (I_s + A_s) - \Delta_+ + \Delta_-}{2}. \end{aligned} \quad (3)$$

The experimental I_g and A_g values are not always available. However, the density functional theory (DFT) method can calculate the gas-phase energy parameters precisely. For example, the calculated I_g (6.29 eV) of ZnPc is in excellent agreement with that of the experimental one (6.39 eV) [39]. We used DFT with the HSE06/spaug-cc-PVTZ level on the GAUSSIAN 16 program and calculated I_g and A_g to be 6.29 eV and 2.00 eV, respectively, for ZnPc, and 7.06 eV and 2.86 eV, respectively, for F_{16} ZnPc. The terms Δ_+ and Δ_- were ignored since the peak energy was used to determine I_s and A_s . Using the experimentally obtained I_s and A_s , D and S are calculated by Eq. (3), and the results are shown in Fig. 4.

Figure 4 shows that D barely increases only by 16 meV for ZnPc and 20 meV for F_{16} ZnPc. This result shows that the relative permittivity in organic molecules changed slightly during the coverage increase. Conversely, S dramatically decreases from -0.17 eV to -0.34 eV when the coverage increases from 0.12 to 0.94 ML for ZnPc. As for F_{16} ZnPc, S increases from 0.29 eV to 0.36 eV, an opposite trend to ZnPc. The variation of S is around 170 meV for ZnPc and 70 meV for F_{16} ZnPc. The systematic error for D and S were estimated from the errors in gas-phase parameters I_s and A_s , and the value is 0.04 eV.

The significantly lower variance of D shows that the molecular density or lattice constant does not affect the coverage-dependent energy levels because the change in lattice constant will drastically change D . We roughly estimated

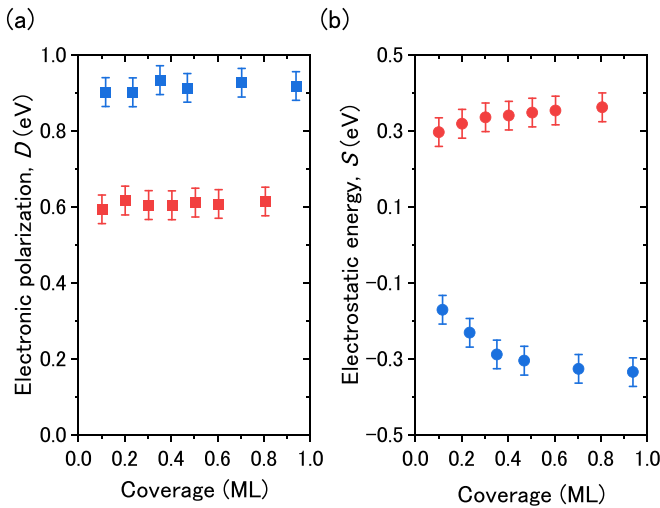


FIG. 4. The coverage dependence of (a) electronic polarization and (b) electrostatic energy of ZnPc (blue) and F₁₆ZnPc (red) until the 1 ML is reached. The error bars are stated in the main text.

the lattice constant of F₁₆ZnPc's D from the charge-induced dipole calculation (the method is shown later) and found that D and S equally depend on the lattice constants (see Supplemental Material Figure S5 [36]). On the other hand, the experimentally obtained D and S for F₁₆ZnPc vary differently (20 meV and 70 meV, respectively) when the coverage increases from 0.1 to 0.8 ML. If the variance of D were caused solely by the change of lattice constant, the change of lattice constant would need to be only 0.1 nm to produce the same variance of experimentally determined D . The variance of experimental S is three times larger than D , which cannot be explained by the change of lattice constants. This indicates that the D and S in this experiment do not come from the effect of the change in the lattice constant.

The higher variance of experimentally determined S compared to D indicates that the coverage-dependent shift of the energy levels is predominately contributed by the electrostatic energy. Furthermore, the opposite trend observed in S of ZnPc and F₁₆ZnPc showed that the electrostatic energy is induced by the charge–permanent quadrupole interaction. This fact is consistent with the calculated quadrupole tensors by DFT with UBL3LYP/cc-PVDZ, where $Q_{xx} = Q_{yy} = 11.534$ and $Q_{zz} = -23.068$ debye Å for ZnPc, and $Q_{xx} = Q_{yy} = -14.442$ and $Q_{zz} = 28.840$ debye Å for F₁₆ZnPc. The magnitudes of the quadrupole tensors are similar while the sign is opposite, explaining the opposite behavior of S between ZnPc and F₁₆ZnPc.

In order to confirm that the coverage dependence of S arises from the sample shape dependence of the electrostatic energy, we calculate D and S from the charge-induced dipole interaction and the charge–quadrupole interaction energies, respectively, on a simplified structural model. Since the film growth in the submonolayer region usually takes the form of an island, the increase of the surface coverage toward one monolayer is associated with an increase in island size. We approximate the island by a disk with a monolayer thickness and a radius R , and a point charge q is placed at the center. We assume that the radius of an island of molecules increases as

the coverage increases without changing the lattice constants. Regarding the response of the neutral molecules to the point charge with a distance r , an induced dipole for D and a permanent quadrupole for S are placed at the center of molecule \mathbf{r} with the polarizability vector $\boldsymbol{\alpha}$ and the quadrupole tensor \mathbf{Q} , respectively.

The potential energy generated by the point charge–induced dipole interaction D and the point charge–permanent quadrupole interaction S can be expressed as (the positive sign stands for the stabilization of the system)

$$D = \frac{1}{2} \sum_n \left(\frac{q}{4\pi\epsilon_0|\mathbf{r}_n|^3} \right)^2 \mathbf{r}_n \boldsymbol{\alpha} \mathbf{r}_n \quad (4a)$$

$$S = - \sum_n q \frac{\mathbf{r}_n \mathbf{Q} \mathbf{r}_n}{4\pi\epsilon_0|\mathbf{r}_n|^5}. \quad (4b)$$

In the monolayer and submonolayer regions, scanning tunneling microscopy (STM) revealed that the phthalocyanines at a temperature less than 70 K form islands with a square lattice or a one-dimensional chain, with the intermolecular distance similar to that in a single crystal [40–42]. Unfortunately, the molecules in the submonolayer region have not been observed at room temperature by STM due to the molecules becoming mobile. Further, a less-disturbing experimental technique such as UPS reported a phase transition of copper-phthalocyanine (CuPc)/HOPG between 80 K and 130 K [43]. As discussed earlier, from the small variance of D , we conclude that the lattice constant can be unchanged across the coverage to the ML. Thus, for the theoretical calculation, we used the lattice constants of a CuPc crystalline film on HOPG for ZnPc single crystal, $a = b = 1.38$ nm, $\gamma = 90.32^\circ$ [44,45], and the reported lattice for face-on orientated F₁₆ZnPc, $a = b = 1.69$ nm, $\gamma = 99.5^\circ$ [46]. The molecular parameters \mathbf{Q} and $\boldsymbol{\alpha}$ are calculated by the DFT (B3LYP/cc-PVDZ) and the Parameterization Method 6 (PM6) method, respectively. The values used for \mathbf{Q} were mentioned earlier, while the values of $\boldsymbol{\alpha}$ for ZnPc were $\alpha_{xx} = \alpha_{yy} = 829.104$ and $\alpha_{zz} = 114.405$ a.u., and for F₁₆ZnPc were $\alpha_{xx} = \alpha_{yy} = 875.382$ and $\alpha_{zz} = 121.439$ a.u. We calculated the D and S values from Eq. (4), as shown in Fig. 5. As predicted, the signs of calculated D are the same for both ZnPc and F₁₆ZnPc, whereas the signs of the calculated S for ZnPc and F₁₆ZnPc are the opposite from each other. The result further confirms that the coverage dependence of S originates from the permanent quadrupole moments, which are opposite between ZnPc and F₁₆ZnPc. However, the relation between the radius of the disk R in the calculation and the coverage is still unclear. We can see that the electrostatic energy calculation reached its plateau around 30 nm. Comparing this with the experimental coverage dependence shown in Fig. 4, the 0.7 ML of the film may composed of islands with only around 20 molecules. Even in the higher coverage region, the small island is consistent with the low-energy electron diffraction (LEED) result, where a two dimensional gas-like structure was observed at less than 0.75 ML of CuPc on Ag(111) [27]. As the molecule–substrate interaction may be smaller between phthalocyanines and HOPG, the molecules should be more mobile, and the gas-phase structure may be maintained at a higher coverage than 0.75 ML. The coverage-dependent work function of

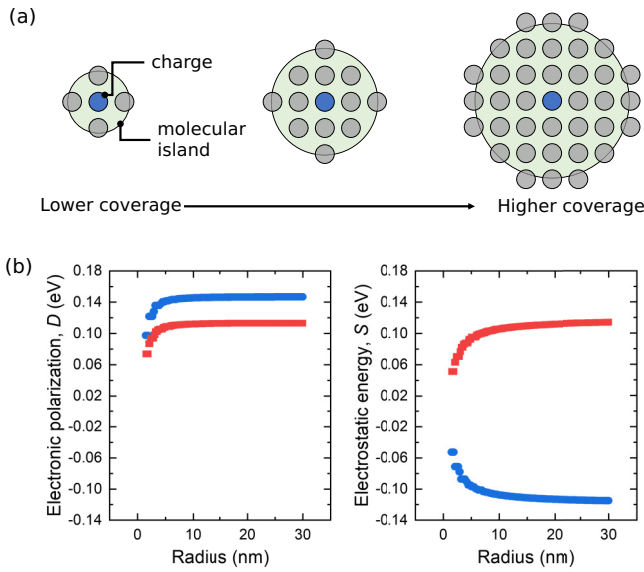


FIG. 5. (a) The disk model for the growing island without a changing lattice constant. (b) The calculated D and S from Eq. (5). The calculations for ZnPc and F₁₆ZnPc are indicated with blue circles and red squares.

CuPc/HOPG saturates around 0.8 ML [47] which is consistent with this prediction.

As shown earlier, we cannot directly relate the radius R in Eq. (4) to the experimental coverage. However, as seen in Fig. 5 and Eq. (4), D and S should depend differently on the radius R because the charge-induced dipole and charge-permanent quadrupole energies are proportional to r^{-4} and r^{-3} , respectively. We further tested the experimental results by using the disk-shaped island model. We assumed a continuum media in the form of a disk and took the interaction between a point charge with induced dipole and permanent quadrupole in their scalar form for D and S , respectively. Then, we integrate over the disk (see Supplemental Materials [36]) to yield ΔD and ΔS values with reference to the infinite radius of R , i.e., fully covered monolayer:

$$\begin{aligned} \Delta D &= \frac{\alpha q^2}{32\epsilon_0^2} \frac{1}{\pi R^2} \propto \frac{1}{N} \\ \Delta S &= \frac{\sqrt{\pi} q Q}{2\epsilon_0} \frac{1}{\sqrt{\pi} R^2} \propto \frac{1}{\sqrt{N}}. \end{aligned} \quad (5)$$

The number of molecules N in a unit area is proportional to the area of the island πR^2 . The coverage is expressed as N/N_0 , where N_0 is the number of atoms of 1 ML (fully covered surface) per the unit area. Equation (5) indicates that ΔD and ΔS follow the power law N^p with the power factors of $p = -1$ and -0.5 , respectively.

Equation (5) is now compared with the experimental results. As shown in Fig. 4, D and S change as a function of coverage and saturate around 0.7 ML. In Fig. 6, we plotted in a log-log plot the absolute values of changes ΔD and ΔS in the experimental D and S with reference to the saturated values, respectively. We found that the experimentally obtained ΔD and ΔS when interpreted as a straight line until 0.7 ML, gives

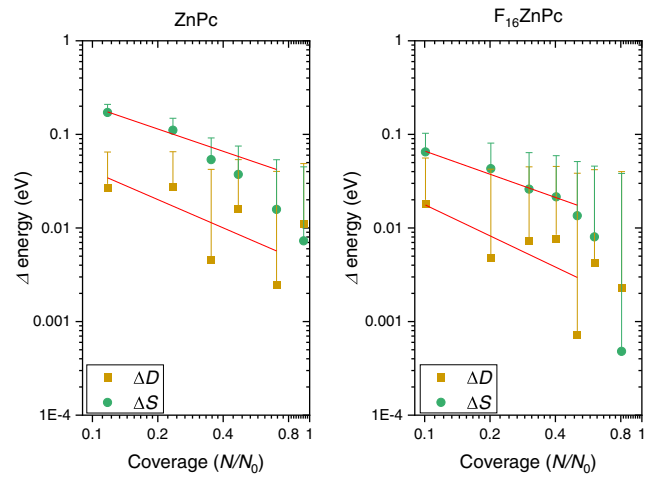


FIG. 6. Experimental electron polarization energy ΔD and electrostatic energy ΔS with reference to the respective value at the monolayer of ZnPc (a) and F₁₆ZnPc (b) versus the coverage. The solid lines are best-fit results in the coverage less than 0.7 ML. The error bars used are the same as in Fig. 4. Only the positive error bar is shown.

a characteristic similar to what is predicted by the power law. The slope of the log-log plot gives the power factor p ; the p of ΔD is -1.0 and -1.1 for ZnPc and F₁₆ZnPc, respectively, while that of ΔS is -0.7 and -0.8 for ZnPc and F₁₆ZnPc, respectively. The values are in good agreement with those predicted by Eq. (5), i.e., $p = -1.0$ for ΔD and $p = -0.5$ for ΔS . The slight difference between the predicted and experimental values is likely due to the actual situation of the sample shape, which may deviate from a perfect circle. Also, we assumed that a point charge is located at the center of the island, which may be a cause of the deviation. After the coverage reached 0.7 ML, the change in D and S drastically decreased (D and S reached its plateau), suggesting that the islands coalesce and make a larger island, which cannot be explained by our disk model.

V. CONCLUSION

We examined both ionization energy and electron affinity of a submonolayer region of ZnPc and F₁₆ZnPc on HOPG by using UPS and LEIPS. We observed a continuous shift of the energy levels, which depends on the coverage and the direction of the quadrupole moment. The electronic polarization and electrostatic energies for both molecules have been quantified. The electronic polarization contribution in the submonolayer region is increased only by 0.02 eV, whereas the electrostatic energies change by 0.17 eV for ZnPc and 0.07 eV for F₁₆ZnPc until the sample reaches its monolayer. The result clearly demonstrates that the coverage-dependent energy shift indeed originates from the electrostatic energy. Further, the results were qualitatively reproduced by the point charge-induced dipole and the point charge-permanent quadrupole interactions calculated for a simplified island model. Remarkably, the coverage-dependent energies follow the power law, where the power factors are in good agreement with the prediction by Eq. (5). We conclude that the

coverage-dependent shifts of the energy levels are predominantly contributed by the electrostatic energy approximated by the charge-permanent quadrupole interaction. This work demonstrates that the observed changes in energy levels can be interpreted as the sample shape-dependent energy levels in organic solids owing to the long-range Coulomb effect. This phenomenon is not only significant to the surface electronic

structure but also relevant to the charge behavior at the interface, e.g., charge separation efficiency in organic photovoltaic cells [48].

ACKNOWLEDGMENT

This work was supported by the Futaba Foundation.

- [1] M. Barret, S. Sanaur, and P. Collot, Inkjet-printed polymer thin-film transistors: Enhancing performances by contact resistances engineering, *Org. Electron.* **9**, 1093 (2008).
- [2] M. Schober, M. Anderson, M. Thomschke, J. Widmer, M. Furno, R. Scholz, B. Lüsse, and K. Leo, Quantitative description of charge-carrier transport in a white organic light-emitting diode, *Phys. Rev. B* **84**, 165326 (2011).
- [3] L. E. Polander, P. Pahnner, M. Schwarze, M. Saalfrank, C. Koerner, and K. Leo, Hole-transport material variation in fully vacuum deposited perovskite solar cells, *APL Mater.* **2**, 081503 (2014).
- [4] D. Veldman, S. C. J. Meskers, and R. A. J. Janssen, The energy of charge-transfer states in electron donor-acceptor blends: Insight into the energy losses in organic solar cells, *Adv. Funct. Mater.* **19**, 1939 (2009).
- [5] J. Widmer, M. Tietze, K. Leo, and M. Riede, Open-circuit voltage and effective gap of organic solar cells, *Adv. Funct. Mater.* **23**, 5814 (2013).
- [6] M. L. Tang and Z. Bao, Halogenated materials as organic semiconductors, *Chem. Mater.* **23**, 446 (2011).
- [7] F. Babudri, G. M. Farinola, F. Naso, and R. Ragni, Fluorinated organic materials for electronic and optoelectronic applications: The role of the fluorine atom, *Chem. Commun.* **10**, 1003 (2007).
- [8] T. Itoh, S. Aomori, and M. Oh-e, Synthesis, properties and FET characteristics of oxygen-based heterocycle dimers 9,9'-bi(benzo[*b*]naphtha[2,1-*d*]furan), *Synth. Met.* **209**, 355 (2015).
- [9] J. Locklin, M. M. Ling, A. Sung, M. E. Roberts, and Z. Bao, High-performance organic semiconductors based on fluorene-phenylene oligomers with high ionization potentials, *Adv. Mater.* **18**, 2989 (2006).
- [10] T. Yamamoto and K. Takimiya, Facile synthesis of highly π -extended heteroarenes, dinaphtho[2,3-*b*:2',3'-*f*]chalcogenopheno[3,2-*b*]chalcogenophenes, and their application to field-effect transistors, *J. Am. Chem. Soc.* **129**, 2224 (2007).
- [11] F. Gutmann and L. E. Lyons, *Organic Semiconductors* (Wiley, New York, 1967).
- [12] N. Sato, K. Seki, and H. Inokuchi, Polarization energies of organic solids determined by ultraviolet photoelectron spectroscopy, *J. Chem. Soc. Faraday Trans. 2* **77**, 1621 (1981).
- [13] S. Duhm, G. Heimel, I. Salzmann, H. Glowatzki, R. L. Johnson, A. Vollmer, J. P. Rabe, and N. Koch, Orientation-dependent ionization energies and interface dipoles in ordered molecular assemblies, *Nat. Mater.* **7**, 326 (2008).
- [14] W. Chen, H. Huang, S. Chen, Y. L. Huang, X. Y. Gao, and A. T. S. Wee, Molecular orientation-dependent ionization potential of organic thin films, *Chem. Mater.* **20**, 7017 (2008).
- [15] G. Heimel, I. Salzmann, S. Duhm, and N. Koch, Design of organic semiconductors from molecular electrostatics, *Chem. Mater.* **23**, 359 (2011).
- [16] H. Yoshida, K. Yamada, J. Tsutsumi, and N. Sato, Complete description of ionization energy and electron affinity in organic solids: Determining contributions from electronic polarization, energy band dispersion, and molecular orientation, *Phys. Rev. B* **92**, 075145 (2015).
- [17] I. Salzmann, S. Duhm, G. Heimel, M. Oehzelt, R. Kniprath, R. L. Johnson, J. P. Rabe, and N. Koch, Tuning the ionization energy of organic semiconductor films: The role of intramolecular polar bonds, *J. Am. Chem. Soc.* **130**, 12870 (2008).
- [18] M. L. Tietze, W. Tress, S. Pfütznner, C. Schünemann, L. Burtone, M. Riede, K. Leo, K. Vandewal, S. Olthof, P. Schulz, and A. Kahn, Correlation of open-circuit voltage and energy levels in zinc-phthalocyanine: C60 bulk heterojunction solar cells with varied mixing ratio, *Phys. Rev. B* **88**, 085119 (2013).
- [19] M. Schwarze, W. Tress, B. Beyer, F. Gao, R. Scholz, C. Poelking, K. Ortstein, A. A. Günther, D. Kasemann, D. Andrienko, and K. Leo, Band structure engineering in organic semiconductors, *Science* **352**, 1446 (2016).
- [20] N. Ueno, Tuning organic band structures with Coulomb interactions: The smooth change of band gaps in blends of organic semiconductors arises from long-range electronic interactions, *Science* **352**, 1395 (2016).
- [21] M. Schwarze, K. S. Schellhammer, K. Ortstein, J. Benduhn, C. Gaul, A. Hinderhofer, L. Perdigon Toro, R. Scholz, J. Kublitski, S. Roland, M. Lau, C. Poelking, D. Andrienko, G. Cuniberti, F. Schreiber, D. Neher, K. Vandewal, F. Ortman, and K. Leo, Impact of molecular quadrupole moments on the energy levels at organic heterojunctions, *Nat. Commun.* **10**, 2466 (2019).
- [22] B. J. Topham and Z. G. Soos, Ionization in organic thin films: Electrostatic potential, electronic polarization, and dopants in pentacene films, *Phys. Rev. B* **84**, 165405 (2011).
- [23] C. Poelking, M. Tietze, C. Elschner, S. Olthof, D. Hertel, B. Baumeier, F. Würthner, K. Meerholz, K. Leo, and D. Andrienko, Impact of mesoscale order on open-circuit voltage in organic solar cells, *Nat. Mater.* **14**, 434 (2015).
- [24] G. D'Avino, L. Muccioli, F. Castet, C. Poelking, D. Andrienko, Z. G. Soos, J. Cornil, and D. Beljonne, Electrostatic phenomena in organic semiconductors: Fundamentals and implications for photovoltaics, *J. Phys. Condens. Matter* **28**, 433002 (2016).
- [25] P. Krüger, Ensemble averaged Madelung energies of finite volumes and surfaces, *Phys. Rev. B* **101**, 205423 (2020).
- [26] T. Sugiyama, T. Sasaki, S. Kera, N. Ueno, and T. Munakata, Intermolecular and interlayer interactions in copper phthalocyanine films as measured with microspot photoemission spectroscopy, *Appl. Phys. Lett.* **89**, 202116 (2006).

- [27] I. Kröger, B. Stadtmüller, C. Stadler, J. Ziroff, M. Kochler, A. Stahl, F. Pollinger, T. L. Lee, J. Zegenhagen, F. Reinert, and C. Kumpf, Submonolayer growth of copper-phthalocyanine on Ag(111), *New J. Phys.* **12**, 083038 (2010).
- [28] H. Yoshida, Near-ultraviolet inverse photoemission spectroscopy using ultra-low energy electrons, *Chem. Phys. Lett.* **539-540**, 180 (2012).
- [29] H. Yoshida, Principle and application of low energy inverse photoemission spectroscopy: A new method for measuring unoccupied states of organic semiconductors, *J. Electron Spectros. Relat. Phenomena* **204**, 116 (2015).
- [30] K. Yamada, S. Yanagisawa, T. Koganezawa, K. Mase, N. Sato, and H. Yoshida, Impact of the molecular quadrupole moment on ionization energy and electron affinity of organic thin films: Experimental determination of electrostatic potential and electronic polarization energies, *Phys. Rev. B* **97**, 245206 (2018).
- [31] A. Sugie, W. Han, N. Shioya, T. Hasegawa, and H. Yoshida, Structure-dependent electron affinities of perylene diimide-based acceptors, *J. Phys. Chem. C* **124**, 9765 (2020).
- [32] Y. Uemura, S. A. Abd-Rahman, S. Yanagisawa, and H. Yoshida, Quantitative analysis of the electrostatic and electronic polarization energies in molecularly mixed films of organic semiconductors, *Phys. Rev. B* **102**, 125302 (2020).
- [33] T. Aihara, S. A. Abd-Rahman, and H. Yoshida, Metal screening effect on energy levels at metal/organic interface: Precise determination of screening energy using photoelectron and inverse-photoelectron spectroscopies, *Phys. Rev. B* **104**, 085305 (2021).
- [34] Y. Harada and H. Ozaki, Penning ionization electron spectroscopy: Its application to surface characterization of organic solids, *Jpn. J. Appl. Phys.* **26**, 1201 (1987).
- [35] Y. Harada, S. Masuda, and H. Ozaki, Electron spectroscopy using metastable atoms as probes for solid surfaces, *Chem. Rev.* **97**, 1897 (1997).
- [36] See Supplemental Material at <http://link.aps.org/supplemental/10.1103/PhysRevB.106.075303> for the determination of a clean HOPG surface by MAES, ML determination by MAES, evaluation of Equation 4, evaluation of Equation 5, and lattice constant dependence of S and D calculation.
- [37] S. Kera, H. Yamane, I. Sakuragi, K. K. Okudaira, and N. Ueno, Very narrow photoemission bandwidth of the highest occupied state in a copper-phthalocyanine monolayer, *Chem. Phys. Lett.* **364**, 93 (2002).
- [38] H. Yoshida, Note: Low energy inverse photoemission spectroscopy apparatus, *Rev. Sci. Instrum.* **85**, 016101 (2014).
- [39] D. Schlettwein, K. Hesse, N. E. Gruhn, P. A. Lee, K. W. Nebesny, and N. R. Armstrong, Electronic energy levels in individual molecules, thin films, and organic heterojunctions of substituted phthalocyanines, *J. Phys. Chem. B* **105**, 4791 (2001).
- [40] K. Walzer and M. Hietschold, STM and STS investigation of ultrathin tin phthalocyanine layers adsorbed on HOPG(0 0 0 1) and Au(1 1 1), *Surf. Sci.* **471**, 1 (2001).
- [41] J. Åhlund, J. Schnadt, K. Nilson, E. Göthelid, J. Schiessling, F. Besenbacher, N. Mårtensson, and C. Puglia, The adsorption of iron phthalocyanine on graphite: A scanning tunnelling microscopy study, *Surf. Sci.* **601**, 3661 (2007).
- [42] K. Nilson, J. Åhlund, B. Brena, E. Göthelid, J. Schiessling, N. Mårtensson, and C. Puglia, Scanning tunneling microscopy study of metal-free phthalocyanine monolayer structures on graphite, *J. Chem. Phys.* **127**, 114702 (2007).
- [43] T. Kataoka, H. Fukagawa, S. Hosoumi, K. Nebashi, K. Sakamoto, and N. Ueno, Observation of a temperature-dependent transition of a copper-phthalocyanine thin film adsorbed on HOPG, *Chem. Phys. Lett.* **451**, 43 (2008).
- [44] S. D. Wang, X. Dong, C. S. Lee, and S. T. Lee, Orderly growth of copper phthalocyanine on highly oriented pyrolytic graphite (HOPG) at high substrate temperatures, *J. Phys. Chem. B* **108**, 1529 (2004).
- [45] D. Schwarz, C. Henneke, and C. Kumpf, Towards functionalization of graphene: In situ study of the nucleation of copper-phthalocyanine on graphene, *New J. Phys.* **18**, 23034 (2016).
- [46] E. Kawabe, D. Yoshimura, K. Kanai, Y. Ouchi, S. Hasegawa, K. K. Okudaira, N. Ueno, and K. Seki, Epitaxial growth of hexadecafluorozincphthalocyanine (F₁₆ZnPc) film deposited on GeS(0 0 1), *Surf. Sci.* **602**, 1328 (2008).
- [47] H. Fukagawa, S. Hosoumi, H. Yamane, S. Kera, and N. Ueno, Dielectric properties of polar-phthalocyanine monolayer systems with repulsive dipole interaction, *Phys. Rev. B* **83**, 085304 (2011).
- [48] C. Poelking and D. Andrienko, Design rules for organic donor-acceptor heterojunctions: Pathway for charge splitting and detrapping, *J. Am. Chem. Soc.* **137**, 6320 (2015).